β-Decay Half-Lives of Neutron-Rich Sulfur to Potassium: Evolution of the $N = 32$ and 34 Subshell Closures below Calcium

Q. B. Zeng,[1,2,3,*] S. Nishimura,[3,†] V. H. Phong,[3] S. Yoshida,[3,4] Z. H. Li,[5] Z. Liu,[1,2] H. Y. Wu,[6,5] C. Y. Fu,[7,3] D. S. Hou,[7] H. Ishiyama,[3] Y. Jang,[8] M. Khandelwal,[9] J. Lee,[8] A. I. Morales,[10,3] T. Niwase,[11] M. Rosenbusch,[3] P. Schury,[12] A. Takamine,[11] M. Wada,[12] W. D. Xian,[7,13] T. T. Yeung,[14,3] A. Estrade,[15] N. Fukuda,[3] L. Guo,[16] Y. Hirayama,[12] B. Hong,[8] S. Iimura,[17] Y. Ito,[18] Y. H. Kim,[19] S. Kimura,[12] J. Lee,[7] X. Ma,[1,2] S. Michimasa,[3] B. Moon,[19,3] Y. F. Niu,[16] J. Park,[19] H. Sakurai,[3] Y. Shimizu,[3] H. Suzuki,[3] H. Takeda,[3] M. Tanaka,[11] Y. Togano,[3] Y. X. Watanabe,[12] J. M. Yap,[7,12] M. Yoshimoto,[3] C. X. Yuan,[13] F. F. Zeng,[1,2] J. Z. Zhang,[5] and X. L. Zhi[16]

[1]*Institute of Modern Physics, Chinese Academy of Sciences, Lanzhou 730000, China*
[2]*School of Nuclear Science and Technology, University of Chinese Academy of Sciences, Beijing 100049, China*
[3]*RIKEN Nishina Center, 2-1 Hirosawa, Wako, Saitama 351-0198, Japan*
[4]*School of Data Science and Management, Utsunomiya University, Mine, Utsunomiya 321-8505, Japan*
[5]*School of Physics and State Key Laboratory of Nuclear Physics and Technology, Peking University, Beijing 100871, China*
[6]*Key Laboratory of Nuclear Data, China Institute of Atomic Energy, Beijing 102413, China*
[7]*Department of Physics, The University of Hong Kong, Pokfulam Road, Hong Kong, China*
[8]*Department of Physics, Korea University, Seoul 02841, Republic of Korea*
[9]*RCNP, Osaka University, Ibaraki, Osaka 567-0047, Japan*
[10]*Instituto de Física Corpuscular, CSIC-Universitat de València, E-46071 València, Spain*
[11]*Kyushu University, Hakozaki, Higashi-ku, Fukuoka 812-8581, Japan*
[12]*KEK Wako Nuclear Science Center, Wako, Saitama 351-0198, Japan*
[13]*Sino-French Institute of Nuclear Engineering and Technology, Sun Yat-Sen University, Zhuhai, 519082, Guangdong, China*
[14]*Department of Physics, The University of Tokyo, 7-3-1 Hongo, Bunkyo, Tokyo 113-0033, Japan*
[15]*Department of Physics and Science of Advanced Materials Program, Central Michigan University, Mount Pleasant, Michigan 48859, USA*
[16]*School of Nuclear Science and Technology, Lanzhou University, Lanzhou 730000, China*
[17]*Department of Physics, Rikkyo University, Toshima, Tokyo 171-8501, Japan*
[18]*Advanced Science Research Center, Japan Atomic Energy Agency, Ibaraki 319-1195, Japan*
[19]*Center for Exotic Nuclear Studies, Institute for Basic Science, Daejeon 34126, Republic of Korea*

(Received 4 June 2025; revised 10 August 2025; accepted 6 October 2025; published 2 December 2025)

The half-lives of 24 isotopes ranging from sulfur to potassium were measured using the ZeroDegree Advanced Decay Station at the Radioactive Isotope Beam Factory, including six of the most neutron-rich —^{47}S, ^{48,49}Cl, ^{51,52}Ar, ^{55}K—for the first time, while the precision for ^{48}Ar and ^{53,54}K was significantly improved. Two prominent features are found: First, a half-life drop at $^{54}K_{35}$ relative to ^{52,53}K, supporting the persistence of the $N = 34$ subshell closure in potassium with $Z = 19$. Second, a high β-decay rate for $^{48}Cl_{31}$ compared to ^{47}Cl and ^{49}Cl, which can be explained by the critical role of the $\nu 1p_{1/2}$ orbital in shell-model calculations. The present calculations indicate that the $N = 32$ subshell gap in chlorine with $Z = 17$ is slightly smaller than that in calcium ($Z = 20$), and the significant excitation across the $N = 32$ subshell in $^{48}Cl_{31}$ is mainly due to strong configuration mixing.

DOI: 10.1103/227j-q7zf

Analogous to electrons in the atom, the atomic nucleus also exhibits shell structures for both protons and neutrons, characterized by significant energy gaps at specific nucleon numbers: $N, Z = 2, 8, 20, 28, 50, 82$, and $N = 126$. Such shell structures were first proposed by Mayer [1] and Haxel *et al.* [2], and were well established for nuclei situated on or near the valley of stability. Recently, significant progress has been made at high-intensity accelerator facilities in providing opportunities to explore properties of nuclei far from the β-stability line. Contemporary experimental investigations have revealed that the magic numbers are not universal throughout the nuclear chart. The traditional closed shells at $N = 8$, 20, and 28 weaken or even disappear in the neutron-rich region [3–10], while a new magic number appears at $N = 16$ near the neutron drip line of oxygen isotopes [11–13].

The quest to map shell evolution in the neutron-rich side has also revealed the possible appearance of new subshell

*Contact author: zengquanbo@impcas.ac.cn
†Contact author: nishimu@ribf.riken.jp

closures at $N = 32$ and 34. Key to this evolution is the proton-neutron (p-n) monopole interaction between the $\pi 0f_{7/2}$ and $\nu 0f_{5/2}$ single-particle orbitals [14,15]. With protons removed from the $\pi 0f_{7/2}$ orbital, the diminished p-n interaction raises the $\nu 0f_{5/2}$ orbital above the $\nu 1p_{1/2}$-$\nu 1p_{3/2}$ spin-orbit partners, forging energy gaps that define these emergent subshell closures at $N = 32$ and 34. Experimentally, the $N = 32$ subshell closure has been proven to exist in Ar [16], Ca [17,18], Ti [19,20], and Cr [21,22] by γ-spectroscopic studies in even-even systems. This shell feature was verified by mass measurements of K [23], Ca [24], Sc [25], and Ti [26] isotopes, although it is significantly weakened in the latter. Intriguingly, charge radius measurements along Ca [27] and K [28,29] isotopic chains show no sign of a minimum or inflection at $N = 32$. This absence of expected shell effect was explained as the halo nature of the $\nu 1p$ orbital [30], which was confirmed in ^{52}Ca [31]. Toward lighter elements, the $N = 32$ shell effect in silicon is predicted to be strong, with $E(2_1^+)$ reaching $\sim$1.8 MeV in ^{46}Si [32]. Until now, the $N = 32$ subshell closure below argon has not been experimentally explored. The $N = 34$ subshell closure has been so far established only in Ca [33–35] and Ar [36]. As indicated by the low-lying structure in ^{55}Sc [37], the systematics of $E(2_1^+)$ and $B(E2; 2_1^+ \rightarrow 0_1^+)$ in Ti [20,38] and Cr [22,39] isotopes, and the mass measurements of Sc, Ti, and V isotopic chains [40–42], a marked weakening of the $N = 34$ subshell closure was inferred for nuclei with $Z > 20$. Given the intermediate position of potassium between calcium and argon, the analogous shell stabilization at $N = 34$ is expected for $Z = 19$. However, no experimental evidence currently available supports this expected shell feature.

In addition to the observables mentioned above, β-decay half-lives can also provide unique shell gap sensitivity [43–45]. Usually, Gamow-Teller (GT) transitions dominate β decay owing to its small $\log ft$ value. In the region of present interest, the low-lying GT transitions are hindered as neutrons and protons occupy the pf and sd shells, respectively, resulting in a considerable contribution of first-forbidden (FF) transitions to the total β-decay rate [46]. Consequently, the systematics of β-decay half-lives along an isotopic chain reflect changes in the strengths of the FF and GT transitions, thereby revealing variations in neutron orbital occupations and the evolution of neutron shell gaps. To date, β-decay half-lives in chlorine are available up to $N = 30$. Interestingly, shell-model (SM) calculations show that the FF transition $\nu 1p_{3/2} \rightarrow \pi 0d_{3/2}$ significantly contributes to the total β-decay rate in ^{44}Cl, indicating the collapse of the $N = 28$ shell [46]. In potassium, although the β-decay half-lives have been measured up to $N = 35$, no significant shell effect was identified at $N = 34$ because of large experimental uncertainties. The present Letter focuses on extending the systematics of β-decay half-lives and improving the precision of previous measurements, aiming to explore shell features at $N = 32$ in chlorine and $N = 34$ in potassium.

The experiment was performed at the Radioactive Isotope Beam Factory (RIBF) of the RIKEN Nishina Center [47,48], in a symbiotic setup with the interaction cross section measurements at focal plane F8 and the mass measurements at F11. Radioactive isotopes were produced by fragmentation of a 345 MeV/u ^{70}Zn primary beam with $\sim$400 pnA intensity bombarding on a 8-mm-thick ^{9}Be target. The BigRIPS in-flight separator [49] was tuned to optimize transmission of ^{55}Ca^{20+} ions. The secondary beam impinged on a target at F8, which was alternately a 1.5 g/cm^2-thick carbon target and a target frame. After the secondary target, both reaction products and the unreacted beams were identified event by event via time-of-flight (TOF), magnetic rigidity, and energy loss measurements, and were transported to F11 through the ZeroDegree Spectrometer (ZDS) [49].

An energy degrader was placed in front of the ZeroDegree Multi-Reflection TOF Mass Spectrograph system [50] to slow down the ions. In total, about 2.3×10^7 ions, which were not captured by the gas catcher, were implanted into the ZeroDegree Advanced Decay Station (ZD-ADS). The particle identification (PID) plot for the implanted ions is shown in Fig. 1. In the current setup, the ZD-ADS comprises an implantation detector, $LaBr_3$ detectors, a neutron TOF array, and a veto detector. The implantation detector, consisting of one segmented plastic scintillator and six position-sensitive photomultiplier tubes, was tilted at a 45° angle to optimize neutron TOF measurements. The plastic scintillator (EJ-228), manufactured by Eljen Technology, has dimensions of $150 \times 100 \times 6$ mm^3 and features a 100×66 pixel array with 4-mm-deep segmentation. The cross section of each pixel is 1.3×1.3 mm^2, leaving a 0.2 mm gap between two neighboring pixels. Six H12700 Hamamatsu 8×8 multi-anode photomultipliers are coupled with the scintillator pad on the nonsegmented side using optical grease. Position information of ions and following β particles was derived

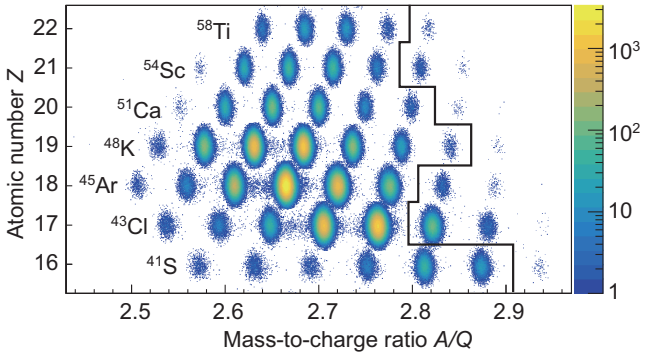

FIG. 1. PID plot of the present experiment identified at ZDS. The newly measured half-lives correspond to nuclei right of the black line.

TABLE I. β-decay half-lives deduced from the present experiment. Experimental results from Ref. [53] are given for comparison.

Nuclide	$T_{1/2}$ (ms)			Nuclide	$T_{1/2}$ (ms)		
	No γ	γ gated[a]	Ref. [53]		No γ	γ gated[a]	Ref. [53]
^{43}S	300 ± 40	⋯	265 ± 13[b]	^{48}Ar	473 ± 4	485 ± 10	415 ± 15
^{44}S	119 ± 8	⋯	100 ± 1[c]	^{49}Ar	252 ± 5	253 ± 12	236 ± 8
^{45}S	75 ± 5	⋯	68 ± 2[d]	^{50}Ar	136 ± 8	134 ± 10	106 ± 6
^{46}S	44 ± 3	⋯	50 ± 8 [e]	^{51}Ar	56 ± 9	⋯	⋯
^{47}S	41 ± 10	⋯	⋯	^{52}Ar	22 ± 10	⋯	⋯
^{44}Cl	700 ± 70	⋯	562 ± 106	^{49}K	1170 ± 40	⋯	1260 ± 50
^{45}Cl	416 ± 28	⋯	413 ± 25[f]	^{50}K	467 ± 9	⋯	472 ± 4
^{46}Cl	238 ± 3	244 ± 27	232 ± 2	^{51}K	372 ± 5	⋯	365 ± 5
^{47}Cl	111 ± 3	117 ± 7	101 ± 5	^{52}K	117 ± 3	⋯	110 ± 4
^{48}Cl	36.5 ± 1.5	⋯	⋯	^{53}K	42.5 ± 2.1	⋯	30 ± 5
^{49}Cl	44 ± 5	⋯	⋯	^{54}K	11.6 ± 2.1	⋯	10 ± 5
^{47}Ar	1410 ± 30	1320 ± 70	1230 ± 30	^{55}K	7 ± 3	⋯	⋯

[a]Gate on γ rays: 1553 keV (in ^{46}Ar) for ^{46,47}Cl; 360 and 1660 keV (in ^{47}K) for ^{47}Ar; 142.7 keV (in ^{48}K) for ^{48}Ar; 91.7 keV (in ^{49}K) for ^{49,50}Ar.
[b]Recently measured $T_{1/2} = 256 \pm 5$ and 250.2 ± 2.5 ms in Ref. [55].
[c]Recently measured $T_{1/2} = 125.5 \pm 2.5$ and 119 ± 6 ms in Ref. [56].
[d]Recently measured $T_{1/2} = 69 \pm 1$ and 74 ± 5 ms in Ref. [55].
[e]Recently measured $T_{1/2} = 41 \pm 4$ ms in Ref. [56].
[f]Recently measured $T_{1/2} = 513 \pm 36$ ms in Ref. [57] and 451 ± 14 ms in Ref. [58].

event by event based on anode signals [51]. The β-detection efficiency extracted from the present data is ∼40% for a 4-mm β-ion spatial correlation radius. Twelve fast-timing $LaBr_3$ detectors from KHALA [52] were arranged in a bundle configuration and mounted on the side of the implantation detector (∼10 cm from its center). The total photopeak efficiency is ∼6% at 200 keV and ∼1% at 1.4 MeV. The neutron detector array was installed above the implantation detector in two layers at a distance of ∼1.1 m. The veto detector was mounted behind the implantation detector and used to reject light particles coming with the beam. This Letter focuses on β-decay half-lives; β-delayed neutron data and neutron detector details will be reported in dedicated publications.

The half-lives of $^{43–47}$S, $^{44–49}$Cl, $^{47–52}$Ar, and $^{49–55}$K were measured in the present experiment, where the half-lives of ^{47}S, ^{48,49}Cl, ^{51,52}Ar, and ^{55}K were determined for the first time, and the precision for ^{48}Ar and ^{53,54}K was significantly improved, as listed in Table I. Additional half-lives for isotopes with $Z \geq 20$, including $^{53–57}$Ca, $^{55–60}$Sc, and $^{58–62}$Ti are provided in the Supplemental Material [54]. The half-life of each isotope was determined by fitting the decay curve with a function that accounted for the parent decay, the exponential growth and decay of the daughter, the granddaughter, and the great-granddaughter nuclei, as well as a constant background, employing the unbinned maximum likelihood fitting procedure. The total error in the present result consists of statistical error and systematic error. The former was determined by the error on the fit parameters, while the latter was introduced to account for the uncertainties of the input parameters, including the β-delayed neutron branching ratios, and the half-lives of the nuclei in the decay chain. The input half-lives and branching ratios were randomly sampled from Gaussian distributions with standard deviations corresponding to their uncertainties, of which the mean values and uncertainties were taken from the literature [53] if available. When the half-lives of the isotopes were measured in this Letter, they were used as input parameters. If there is no experimental information on β-delayed neutron emission probability, uniform distribution was used to generate a random number as branching ratio. In some cases, β-decay curves gated on β-delayed γ rays were analyzed to verify the results, where the sum of an exponential decay and a constant background

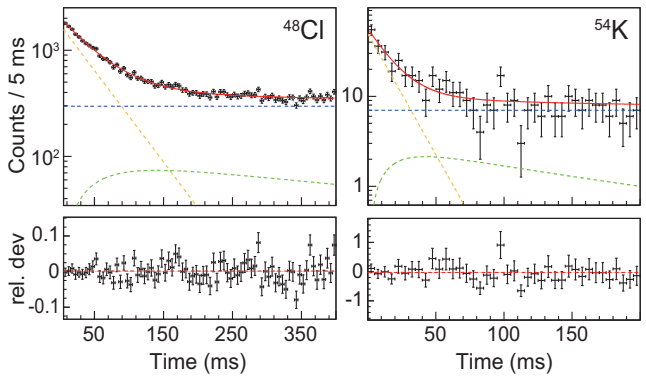

FIG. 2. Best fits to the decay curves for ^{48}Cl and ^{54}K. The red solid line is the total fit; the orange dashed line shows the parent decay; the green dashed line is the sum of contributions from $\beta 0n$, $\beta 1n$, and $\beta 2n$ daughters. The relative deviation is presented below the decay curve.

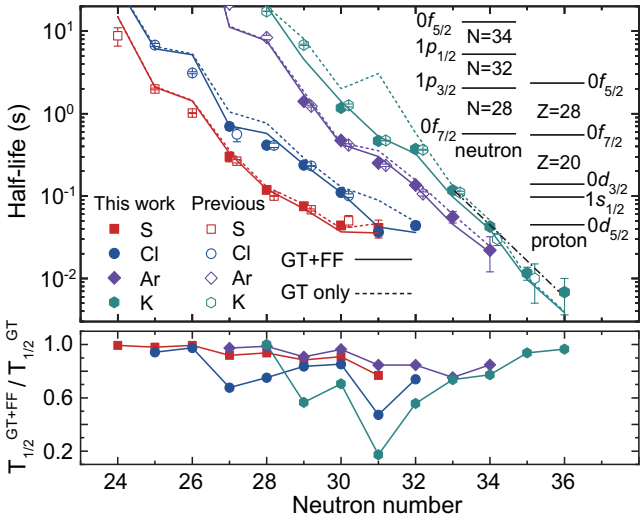

FIG. 3. Upper: the systematics of β-decay half-lives for neutron-rich S, Cl, Ar, and K isotopic chains as a functions of the neutron number. The filled symbols represent the experimental half-lives obtained in the present experiment without γ tagging, while half-lives from the literature [53] are shown with open symbols. The solid (dashed) lines show the predicted half-lives including GT and FF (only GT) transitions from the present SM calculations. These predictions correspond to the experimental data shown in the same colors. The black dash-dotted reference line is drawn to show the drop at ^{54}K, relative to the half-lives of ^{52,53}K. The relevant neutron and proton orbitals are also shown. Lower: ratio of the predicted half-life with the FF and GT transitions to the one with the GT transition only.

was used to fit the decay curve. Figure 2 shows the decay curves for ^{48}Cl and ^{54}K, along with the fitting functions and the relative deviations.

The upper panel of Fig. 3 shows the systematic trends in β-decay half-lives along S, Cl, Ar, and K isotopic chains. For comparison, the literature values from Ref. [53] are also presented with open symbols. With our new results, a half-life drop at $N = 35$ relative to $N = 33$ and 34 is observed in potassium for the first time, which can be explained by the $N = 34$ subshell closure. For the K isotopes with $28 < N \leq 34$, the last neutron is predominantly situated in the $1p$ orbital if the $N = 34$ subshell closure exists; consequently, the β-decay processes are dominated by the high-lying GT transitions and the low-lying FF transitions $\nu 1p \rightarrow \pi 1s$ and $\nu 1p \rightarrow \pi 0d$. At $N = 35$, the last neutron abruptly occupies the $\nu 0f_{5/2}$ orbital, making the GT decay channel $\nu 0f_{5/2} \rightarrow \pi 0f_{7/2}$ accessible. In this case, the excitation energy of the populated state is much lower than that in other GT transition channels. Additionally, the presence of the $N = 34$ subshell gap would result in an increase in Q_β and thus accelerate the β-decay rates. It is worth noting that the $\Delta J^\pi = 0^-$ FF transition can be enhanced by the meson-exchange contribution to the matrix element of γ_5 [59,60], significantly shortening the β-decay half-lives. For example, the $\log ft$ of the $^{50}\mathrm{K}(0_1^-) \rightarrow {}^{50}\mathrm{Ca}(0_1^+)$ transition was measured to be 5.89 ± 0.06 with a branching ratio of $61.0 \pm 7.4\%$ [61], and the $^{52}\mathrm{K}(2_1^-) \rightarrow {}^{52}\mathrm{Ca}(2_1^+)$ decay was also found to be strengthened with a $\log ft$ of 5.7 ± 0.2 [62]. A remarkable reduction of β-decay half-lives by enhanced FF transitions is expected to occur in $\nu 1p_{1/2} \rightarrow \pi 1s_{1/2}$, $\nu 1p_{3/2} \rightarrow \pi 0d_{3/2}$, and $\nu 0f_{5/2} \rightarrow \pi 0d_{5/2}$ transitions. However, the latter would contribute less, rendering the half-life drop at $N = 35$ less significant.

The other novel feature is the dramatically enhanced total β-decay strength of ^{48}Cl, as demonstrated by its shorter half-life compared to ^{47}Cl and ^{49}Cl. It is reasonable to assume that the last (31st) neutron in ^{48}Cl mainly occupies the $1p$ orbital, and thus two mechanisms are likely responsible for the acceleration of the total β-decay rate. The first is the accelerating GT transition, which can be achieved by, for instance, lowering the $\pi 1p$ and $\pi 0f$ orbitals to increase the Q_β. The total decay rate can also be enhanced by the low-lying $\Delta J^\pi = 0^-$ FF transition with a small $\log ft$ value, as demonstrated in the β-decay processes of ^{50}K [61] and ^{52}K [62].

In order to further explain the experimental results, SM calculations using the SDPFSDG-MU effective interaction [46] and Q_β from AME2020 [63] were performed with the KSHELL code [64,65]. For every isotope measured in this Letter, the SM calculations predict a few low-lying levels, each with a calculated β-decay half-life. One of the theoretical half-lives is adopted for comparison with the measured value: If the ground state spin-parity (J^π) has been experimentally established, but cannot be reproduced by the SM calculations, the theoretical half-life of the low-lying state with the same J^π is adopted. For nuclides with experimentally unknown ground state J^π, the predicted low-lying state with a half-life closest to the experimental value is taken as the ground state.

As shown in the upper panel of Fig. 3, the SDPFSDG-MU effective interaction demonstrates powerful predictive ability in this region. Especially, the present calculations describe the FF transition very well by employing an effective operator. One example is the β decay of ^{50}K, where the $\log ft$ of the $^{50}\mathrm{K}(0_1^-) \rightarrow {}^{50}\mathrm{Ca}(0_1^+)$ transition was measured to be 5.89 ± 0.06 [61], which is well reproduced as 5.84 in our calculations. In addition to ^{50}K, FF transitions also play a significant role in the β decay of other K isotopes with $28 < N \leq 34$. Beyond $N = 34$, the contributions from the FF transitions markedly decrease and the GT transitions dominate the total β-decay rates, as illustrated in the lower panel of Fig. 3. Meanwhile, one can also find that the predicted GT transition half-life of ^{54}K is considerably shorter compared to $^{51-53}$K. The behavior of both GT and FF transitions reflects a rapid change in orbital occupation for the last neutron from $1p$ to $0f_{5/2}$, indicating the presence of the $N = 34$ subshell closure. In the present calculations, the $N = 34$ subshell gap is predicted to be ~4.2 MeV, similar to that in ^{54}Ca (~4.5 MeV), although the latter overestimates the experimental value [34]. The size of the $N = 34$ gap is defined here as the empirical

TABLE II. The present SM results for ^{48}Cl. Spin-parity J^π, excitation energy, orbital occupation numbers, and β-decay half-lives of four low-lying states are listed.

J^π	E_x (keV)	$\nu 1p_{3/2}$	$\nu 1p_{1/2}$	$T_{1/2}^{\mathrm{GT+FF}}$ (ms)	$T_{1/2}^{\mathrm{GT}}$ (ms)
0^-	78	2.45	0.98	42	89
1^-	119	2.62	0.85	59	98
2^-	0	2.79	0.49	83	119
3^-	57	2.96	0.39	103	141

two-neutron shell gap $\Delta S_{2n}(N) = S_{2n}(N) - S_{2n}(N+2)$ [66], where S_{2n} denotes the two-neutron separation energy.

Theoretically, it is difficult to predict the ground state J^π of odd-odd nuclei because of the dense low-lying states. Experimental information on the β decay is crucial in determining the J^π of the ground state and thereby to test effective interactions. So far, the J^π of the ground state in ^{48}Cl has not been established. Our calculations suggest a 2^- ground state with $T_{1/2} = 83$ ms, much longer than the experimental value of 36.5 ± 1.5 ms. Above the 2^- state, three low-lying states with different β-decay half-lives and configurations are predicted, as listed in Table II. We found that the β-decay half-life of the 78-keV 0^- state is closest to our measured value and reproduces the systematic trend in the upper panel of Fig. 3. This state strongly feeds the ground state in ^{48}Ar through a FF transition with a log ft of 5.51 and a branching ratio of 43% in our calculations. The primary configuration of this 0^- state is predicted to be $\pi 1s_{1/2}^{-1}\nu 1p_{1/2}^{1}$, in contrast to the $\pi 0d_{3/2}^{-1}\nu 1p_{3/2}^{1}$ 0^- ground state in the isotone ^{50}K [61]. Our calculations demonstrate that three components contribute to the $^{48}\mathrm{Cl}(0_1^-) \to {}^{48}\mathrm{Ar}(0_1^+)$ and $^{50}\mathrm{K}(0_1^-) \to {}^{50}\mathrm{Ca}(0_1^+)$ transitions: $\nu 0f_{5/2} \to \pi 0d_{5/2}$, $\nu 1p_{3/2} \to \pi 0d_{3/2}$, and $\nu 1p_{1/2} \to \pi 1s_{1/2}$, which are all dominated by the timelike part of the rank-0 axial current M_0^T. As shown in Fig. 4, the $0_1^- \to 0_1^+$ transition in ^{50}K is predominantly driven by $\nu 1p_{3/2} \to \pi 0d_{3/2}$, but by $\nu 1p_{1/2} \to \pi 1s_{1/2}$ in ^{48}Cl.

The above analysis indicates the $\nu 1p_{1/2}$ orbital plays a crucial role in the β decay of ^{48}Cl, leading to a natural conjecture that the $N = 32$ subshell closure significantly erodes in chlorine compared with potassium. The $\Delta S_{2n}(N = 32)$ values extracted from the present SM calculations are 3.8 (Ca), 3.7 (K), 2.6 (Ar), and 2.2 (Cl) MeV, with the Ca and K results comparable to the experimental values [23,24]. The small $\Delta S_{2n}(N = 32)$ in chlorine is consistent with the crucial role of the $\nu 1p_{1/2}$ orbital in the ^{48}Cl β-decay process. However, the $N = 32$ gap shows only a slight decrease: 3.9 (Ca), 3.6 (K), 3.3 (Ar), and 3.2 (Cl) MeV, where the shell gap is defined as the difference in energy between $\nu 1p_{3/2}^4$ and $\nu(1p_{3/2}^2 1p_{1/2}^2)$ configurations in the $N = 32$ isotones. The discrepancy between these two quantities comes from the configuration mixing—in the $\Delta S_{2n}(N)$ approach, fragmentation of the wave function is fully considered, while it is significantly reduced by constraint of neutron orbital occupation in the second scheme, which more accurately describes the shell gap. The present SM calculations show that ground states in ^{52}Ca and ^{51}K are dominated by $\pi(0d_{3/2}^4 1s_{1/2}^2) \otimes \nu(1p_{3/2}^4)$ (87%) and $\pi(0d_{3/2}^3 1s_{1/2}^2) \otimes \nu(1p_{3/2}^4)$ (75%), respectively; while the largest components $\pi(0d_{3/2}^2 1s_{1/2}^2) \otimes \nu(1p_{3/2}^4)$ in ^{50}Ar and $\pi(d_{3/2}^1 1s_{1/2}^2) \otimes \nu(1p_{3/2}^4)$ in ^{49}Cl are only 46% and 41%, respectively. The $N = 32$ shell effect remains strong in Ca and K with their relatively pure configurations, but weakens drastically in Ar and Cl because of strong configuration mixing. Such quenching of the shell effect also manifests in the low $E(2_1^+)$ of 1178(18) keV in ^{50}Ar [16] and the 893(75) keV reduction of $1/2_1^- - 3/2_1^-$ energy splitting in ^{47}Ar compared to ^{49}Ca [67,68].

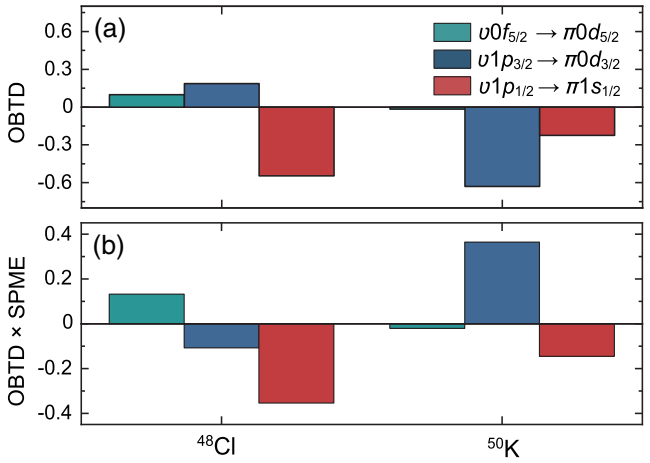

FIG. 4. The components of the $0_1^- \to 0_1^+$ FF transitions in ^{48}Cl and ^{50}K, represented by (a) one-body transition densities (OBTDs) and (b) the products of OBTDs and M_0^T-related single particle matrix elements (SPMEs).

In summary, we measured the half-lives of 24 neutron-rich isotopes ranging from sulfur to potassium using the ZD-ADS at the RIBF. The half-lives of ^{47}S, ^{48,49}Cl, ^{51,52}Ar, and ^{55}K were determined for the first time, and the half-lives of ^{48}Ar and ^{53,54}K were remeasured with notably higher precision. Two prominent features are observed and discussed with the help of SM calculations using the SDPFSDG-MU effective interaction. In the first case, the half-life drop at ^{54}K provides the first experimental confirmation of the $N = 34$ subshell closure in K isotopes, in agreement with theoretical predictions. The second case is the significant enhancement of the total β-decay rate in ^{48}Cl, which can be accounted for by the crucial role of the $\nu 1p_{1/2}$ orbital. The SM calculations indicate that the $N = 32$ subshell gap in Cl is slightly smaller than that in Ca, and the significant excitation across the $N = 32$ subshell in ^{48}Cl is mainly due to strong configuration mixing. Intriguingly, strong shell effects at $N = 32$ and 34 are predicted in Si isotopes with $E(2_1^+)$ of ~1.8 MeV in ^{46}Si and ~3 MeV in ^{48}Si [32], encouraging further experiments to study the evolution of these subshell closures in more exotic regions.

Acknowledgments—This work was carried out at the RIBF operated by RIKEN Nishina Center, RIKEN, and CNS, University of Tokyo. We acknowledge Korea University for the loan of the KHALA detectors. S. N. acknowledges the JSPS KAKENHI (Grants No. 17H06090, No. 20H05648, No. 22H04946, No. 25H01273) and the RIKEN programs (r-EMU and RiNA-Net). B. M. acknowledges a support from Institute for Basic Science of the Republic of Korea under Grant No. IBS-R031-Y1. Y. H. K. and J. P. acknowledge the Grant No. IBS-R031-D1. T. T. Y. acknowledges support from Grant-in-Aid for JSPS Fellows Grant No. 23KJ0727; JSR Fellowship, the University of Tokyo; and Forefront Physics and Mathematics Program to Drive Transformation (FoPM), a World-Leading Innovative Graduate Study (WINGS) Program, the University of Tokyo. This work was supported by the National Research Foundation of Korea (NRF) grant funded by the Korea government (MSIT) (2018R1A5A1025563, RS-2024-00333673, RS-2024-00436392), by JSPS KAKENHI Grants No. JP22K14030 and No. 25H01511, by the Spanish Ministerio de Ciencia, Innovación y Universidades (CAS22/00114, CNS2023-144871, and PID2023-150056NB-C41), Generalitat Valenciana (CISEJI/2022/25), by the National Natural Science Foundation of China (Grant No. 12135004), and by the National Natural Science Foundation of China under Grant No. 12475129. This research was partly conducted using the FUJITSU Supercomputer PRIMEHPC FX1000 and FUJITSU Server PRIMERGY GX2570 (Wisteria/BDEC-01) at the Information Technology Center, The University of Tokyo.

Data availability—The data that support the findings of this article are not publicly available because of legal restrictions preventing unrestricted public distribution. The data are available from the authors upon reasonable request.

[1] M. G. Mayer, Phys. Rev. **75**, 1969 (1949).
[2] O. Haxel, J. H. D. Jensen, and H. E. Suess, Phys. Rev. **75**, 1766 (1949).
[3] A. Navin *et al.*, Phys. Rev. Lett. **85**, 266 (2000).
[4] H. Iwasaki *et al.*, Phys. Lett. B **481**, 7 (2000).
[5] H. Iwasaki *et al.*, Phys. Lett. B **491**, 8 (2000).
[6] S. Shimoura *et al.*, Phys. Lett. B **560**, 31 (2003).
[7] C. Thibault, R. Klapisch, C. Rigaud, A. M. Poskanzer, R. Prieels, L. Lessard, and W. Reisdorf, Phys. Rev. C **12**, 644 (1975).
[8] T. Motobayashi, Y. Ikeda, K. Ieki, M. Inoue, N. Iwasa, T. Kikuchi, M. Kurokawa, S. Moriya, S. Ogawa, H. Murakami, S. Shimoura, Y. Yanagisawa, T. Nakamura, Y. Watanabe, M. Ishihara, T. Teranishi, H. Okuno, and R. Casten, Phys. Lett. B **346**, 9 (1995).
[9] B. Bastin *et al.*, Phys. Rev. Lett. **99**, 022503 (2007).
[10] S. Takeuchi *et al.*, Phys. Rev. Lett. **109**, 182501 (2012).
[11] A. Ozawa, T. Kobayashi, T. Suzuki, K. Yoshida, and I. Tanihata, Phys. Rev. Lett. **84**, 5493 (2000).
[12] R. Kanungo *et al.*, Phys. Rev. Lett. **102**, 152501 (2009).
[13] C. R. Hoffman *et al.*, Phys. Rev. Lett. **100**, 152502 (2008).
[14] T. Otsuka, T. Suzuki, R. Fujimoto, H. Grawe, and Y. Akaishi, Phys. Rev. Lett. **95**, 232502 (2005).
[15] T. Otsuka, Phys. Scr. T **152**, 014007 (2013).
[16] D. Steppenbeck *et al.*, Phys. Rev. Lett. **114**, 252501 (2015).
[17] A. Huck, G. Klotz, A. Knipper, C. Miehé, C. Richard-Serre, G. Walter, A. Poves, H. L. Ravn, and G. Marguier, Phys. Rev. C **31**, 2226 (1985).
[18] A. Gade, R. V. F. Janssens, D. Bazin, R. Broda, B. A. Brown, C. M. Campbell, M. P. Carpenter, J. M. Cook, A. N. Deacon, D.-C. Dinca, B. Fornal, S. J. Freeman, T. Glasmacher, P. G. Hansen, B. P. Kay, P. F. Mantica, W. F. Mueller, J. R. Terry, J. A. Tostevin, and S. Zhu, Phys. Rev. C **74**, 021302(R) (2006).
[19] R. Janssens *et al.*, Phys. Lett. B **546**, 55 (2002).
[20] D.-C. Dinca *et al.*, Phys. Rev. C **71**, 041302(R) (2005).
[21] J. Prisciandaro, P. Mantica, B. Brown, D. Anthony, M. Cooper, A. Garcia, D. Groh, A. Komives, W. Kumarasiri, P. Lofy, A. Oros-Peusquens, S. Tabor, and M. Wiedeking, Phys. Lett. B **510**, 17 (2001).
[22] A. Bürger *et al.*, Phys. Lett. B **622**, 29 (2005).
[23] M. Rosenbusch *et al.*, Phys. Rev. Lett. **114**, 202501 (2015).
[24] F. Wienholtz *et al.*, Nature (London) **498**, 346 (2013).
[25] X. Xu *et al.*, Phys. Rev. C **99**, 064303 (2019).
[26] E. Leistenschneider *et al.*, Phys. Rev. Lett. **120**, 062503 (2018).
[27] R. F. Garcia Ruiz *et al.*, Nat. Phys. **12**, 594 (2016).
[28] K. Kreim, M. Bissell, J. Papuga, K. Blaum, M. De Rydt, R. Garcia Ruiz, S. Goriely, H. Heylen, M. Kowalska, R. Neugart, G. Neyens, W. Nörtershäuser, M. Rajabali, R. Sánchez Alarcón, H. Stroke, and D. Yordanov, Phys. Lett. B **731**, 97 (2014).
[29] Á. Koszorús *et al.*, Nat. Phys. **17**, 439 (2021).
[30] J. Bonnard, S. M. Lenzi, and A. P. Zuker, Phys. Rev. Lett. **116**, 212501 (2016).
[31] M. Enciu *et al.*, Phys. Rev. Lett. **129**, 262501 (2022).
[32] Y. Utsuno, T. Otsuka, Y. Tsunoda, N. Shimizu, M. Honma, T. Togashi, and T. Mizusaki, in *Proceedings of the Conference on Advances in Radioactive Isotope Science (ARIS2014)* (Journal of the Physical Society of Japan, 2015), 10.7566/jpscp.6.010007.
[33] D. Steppenbeck *et al.*, Nature (London) **502**, 207 (2013).
[34] S. Michimasa *et al.*, Phys. Rev. Lett. **121**, 022506 (2018).
[35] S. Chen *et al.*, Phys. Rev. Lett. **123**, 142501 (2019).
[36] H. N. Liu *et al.*, Phys. Rev. Lett. **122**, 072502 (2019).
[37] D. Steppenbeck *et al.*, Phys. Rev. C **96**, 064310 (2017).
[38] H. Suzuki *et al.*, Phys. Rev. C **88**, 024326 (2013).
[39] S. Zhu *et al.*, Phys. Rev. C **74**, 064315 (2006).
[40] E. Leistenschneider, E. Dunling, G. Bollen, B. A. Brown, J. Dilling, A. Hamaker, J. D. Holt, A. Jacobs, A. A. Kwiatkowski, T. Miyagi, W. S. Porter, D. Puentes, M. Redshaw, M. P. Reiter, R. Ringle, R. Sandler, C. S. Sumithrarachchi, A. A. Valverde, and I. T. Yandow (The LEBIT Collaboration and the TITAN Collaboration), Phys. Rev. Lett. **126**, 042501 (2021).
[41] W. S. Porter *et al.*, Phys. Rev. C **106**, 024312 (2022).
[42] S. Iimura *et al.*, Phys. Rev. Lett. **130**, 012501 (2023).

[43] O. Sorlin *et al.*, Phys. Rev. C **47**, 2941 (1993).
[44] Z. Y. Xu *et al.*, Phys. Rev. Lett. **113**, 032505 (2014).
[45] X. Zhang, Z. Ren, Q. Zhi, and Q. Zheng, J. Phys. G **34**, 2611 (2007).
[46] S. Yoshida, Y. Utsuno, N. Shimizu, and T. Otsuka, Phys. Rev. C **97**, 054321 (2018).
[47] Y. Yano, Nucl. Instrum. Methods Phys. Res., Sect. B **261**, 1009 (2007).
[48] H. Sakurai, Nucl. Phys. **A805**, 526c (2008).
[49] T. Kubo, D. Kameda, H. Suzuki, N. Fukuda, H. Takeda, Y. Yanagisawa, M. Ohtake, K. Kusaka, K. Yoshida, N. Inabe, T. Ohnishi, A. Yoshida, K. Tanaka, and Y. Mizoi, Prog. Theor. Exp. Phys. **2012**, 03C003 (2012).
[50] M. Rosenbusch *et al.*, Nucl. Instrum. Methods Phys. Res., Sect. A **1047**, 167824 (2023).
[51] Q. Zeng, V. Phong, and S. Nishimura, RIKEN Accel. Prog. Rep. 136 (2024).
[52] B. Moon, J. Lee, Y. Jang, B. Hong, S. Ahn, S. Bae, K. Hahn, Y. Kim, and J. Park, Nucl. Instrum. Methods Phys. Res., Sect. B **541**, 253 (2023).
[53] F. Kondev, M. Wang, W. Huang, S. Naimi, and G. Audi, Chin. Phys. C **45**, 030001 (2021).
[54] See Supplemental Material at http://link.aps.org/supplemental/10.1103/227j-q7zf for the half-lives of isotopes with $Z \geq 20$ measured in the present experiment.
[55] V. Tripathi *et al.*, Phys. Rev. C **109**, 044320 (2024).
[56] V. Tripathi *et al.*, Phys. Rev. C **106**, 064314 (2022).
[57] S. Bhattacharya *et al.*, Phys. Rev. C **108**, 024312 (2023).
[58] I. Cox *et al.*, Phys. Rev. Lett. **132**, 152503 (2024).
[59] K. Kubodera, J. Delorme, and M. Rho, Phys. Rev. Lett. **40**, 755 (1978).
[60] P. Guichon, M. Giffon, J. Joseph, R. Laverrière, and C. Samour, Z. Phys. A **285**, 183 (1978).
[61] P. Baumann, M. Bounajma, F. Didierjean, A. Huck, A. Knipper, M. Ramdhane, G. Walter, G. Marguier, C. Richard-Serre, and B. A. Brown, Phys. Rev. C **58**, 1970 (1998).
[62] F. Perrot *et al.*, Phys. Rev. C **74**, 014313 (2006).
[63] M. Wang, W. Huang, K. F. G., A. G., and S. Naimi, Chin. Phys. C **45**, 030003 (2021).
[64] N. Shimizu, Nuclear shell-model code for massive parallel computation, arXiv:1310.5431.
[65] N. Shimizu, T. Mizusaki, Y. Utsuno, and Y. Tsunoda, Comput. Phys. Commun. **244**, 372 (2019).
[66] D. Lunney, J. M. Pearson, and C. Thibault, Rev. Mod. Phys. **75**, 1021 (2003).
[67] L. Gaudefroy *et al.*, Phys. Rev. Lett. **97**, 092501 (2006).
[68] A. Signoracci and B. A. Brown, Phys. Rev. Lett. **99**, 099201 (2007).